Construction, MD Simulation, and Hydrodynamic Validation of an All-Atom Model of a Monoclonal IgG Antibody

J. Paul Brandt,[†‡] Thomas W. Patapoff,[†] and Sergio R. Aragon[‡*]
[†]Department of Early Stage Pharmaceutical Development, Genentech, South San Francisco, California; and [‡]Department of Chemistry and Biochemistry, San Francisco State University, San Francisco, California

ABSTRACT At 150 kDa, antibodies of the IgG class are too large for their structure to be determined with current NMR methodologies. Because of hinge-region flexibility, it is difficult to obtain atomic-level structural information from the crystal, and questions regarding antibody structure and dynamics in solution remain unaddressed. Here we describe the construction of a model of a human IgG1 monoclonal antibody (trastuzumab) from the crystal structures of fragments. We use a combination of molecular-dynamics (MD) simulation, continuum hydrodynamics modeling, and experimental diffusion measurements to explore antibody behavior in aqueous solution. Hydrodynamic modeling provides a link between the atomic-level details of MD simulation and the size- and shape-dependent data provided by hydrodynamic measurements. Eight independent 40 ns MD trajectories were obtained with the AMBER program suite. The ensemble average of the computed transport properties over all of the MD trajectories agrees remarkably well with the value of the translational diffusion coefficient obtained with dynamic light scattering at 20°C and 27°C, and the intrinsic viscosity measured at 20°C. Therefore, our MD results likely represent a realistic sampling of the conformational space that an antibody explores in aqueous solution.

INTRODUCTION

Early studies of antibodies were able to establish, using the results of classical hydrodynamic methods, optical rotatory dispersion, and fluorescence anisotropy, that antibodies of the IgG class have a molecular mass of ~150 kDa, exhibit a Y-shaped structure composed of three globular domains linked together by a flexible hinge, and are mostly composed of β-sheets (1,2). Later studies using crystallography were able to definitively provide high-resolution details of the domain structure of antibodies (3). However, there are only a few cases in which a whole antibody's structure has been successfully resolved in atomic detail (4–6). Although they are among the most studied of all macromolecules, there is still a lack of information regarding the structure and dynamics of whole antibodies in the literature.

Obtaining crystals of full-length antibodies that yield atomic-level detail for the entire structure has proved to be an exceedingly difficult task. Among the few success stories in this regard (5,6) are reports of a naturally hinge-deleted antibody (7) and a mouse IgG2a antibody (4) that appears in its crystals to have antigenic activity toward an epitope on its own Fc domain, a feature that is likely responsible for the molecule's orderly crystallization. These successes in particular, due to the exceptional features of the antibody in each case, confirm that the flexibility conferred by the hinge region is the source of the difficulty of crystallizing antibodies. On the other hand, fragments of antibodies are fairly readily crystallized, and many instances of antibody fragments with high-resolution detail can be found in the Protein Data Bank (PDB) (3).

NMR is the method of choice to investigate the structure and dynamics of molecules in solution, but currently the molecule size limit that can be studied is ~35 kDa (8). In the study described in this work, we use a combination of all-atom and continuum mechanics-based modeling techniques along with experimental hydrodynamic methods to establish a methodology that is capable of filling in details of antibodies' aqueous phase structure and dynamics that are otherwise not accessible.

A number of studies in the literature determined whole antibody structure using a combination of solution phase data and modeling (9–14). Boehm et al. (9), Furtado et al. (10), and Sun et al. (11) used x-ray and neutron scattering along with constrained modeling to match measured scattering data and produce very detailed families of models of IgA, IgD, and IgG structure. Additionally, a body of work by Longman et al. (12) and Lu et al. (13,14) employing coarse-grained hydrodynamic bead modeling of rigid ellipsoidal subunits, with sizes and axial ratios determined with data from the crystal structures of actual antibody domains, has identified single conformations for IgG structures that possess properties consistent with those measured experimentally. Although some success can be achieved in distinguishing antibodies that differ significantly in the length of their hinge (13,14), these models do not take the intrinsic flexibility of the antibody into account and thus provide little insight into its fluctuating structure in solution. In contrast, our approach uses an all-atom model of the antibody whose structure is modeled by explicit solvent molecular-dynamics (MD) simulation. Once we have validated such a construction against experimental data, we will be able to extract significant structural and dynamical information from the MD trajectories. With similar goals in mind, Chennamsetty

Submitted January 13, 2010, and accepted for publication May 3, 2010.
*Correspondence: aragons@sfsu.edu
Editor: Alexandre M. J. J. Bonvin.

0006-3495/10/08/0905/9 $2.00
doi: 10.1016/j.bpj.2010.05.003

et al. (15,16) recently investigated antibody solution phase properties using protocols for model building and simulation similar to those employed in our study.

The work described here includes the construction of an all-atom model of a recombinant humanized anti-HER2 IgG1 monoclonal antibody, trastuzumab (Genetech, South San Francisco, CA) (17,18). Using MD simulation, the structure, as initially pieced together from the crystal structures of fragments, was equilibrated in silico in an aqueous solution and allowed to relax into a conformation that is more likely characteristic of the antibody it represents when in actual aqueous solution. Multiple MD trajectories were started using the result of the initial trajectory as their starting structure. Each of the trajectories produced represents a distinct exploration of the phase space accessible from the common starting structure. To evaluate whether the structures generated in the series of MD simulations are possibly representative of actual conformations of human IgG1 samples in solution, we compute the transport properties of the structures using a precise boundary element hydrodynamic modeling technique. Since the hydrodynamic modeling technique used computes the properties of a particle based on the dimensions and topology of its solvent-accessible surface, it is an ideal technique to analyze the results of MD simulations of large, flexible molecules such as antibodies, whose transport properties are expected to fluctuate as they sample their available conformational space. Such an analysis is very useful because the results are directly comparable to those obtained with experimental hydrodynamic methods.

In this work, we show that accurate hydrodynamic computations can be used to validate atomistic structural data against experimental hydrodynamic data and thus evaluate the quality of the specific AMBER force fields used in this study. Therefore, in addition to presenting the initial results from our studies of the solution phase structure and dynamics of a human IgG1 monoclonal antibody, we also describe a methodology for the in silico construction of an antibody for which there is no complete crystal structure. One of the major findings of this work is that the presently available force fields are accurate enough to arrive at realistic solution structures even after separate domain pieces are put together with multiple mutations to reach a specific amino acid sequence of interest. This technique should be broadly applicable to various classes of antibodies whose crystal structures are lacking.

MATERIALS AND METHODS

Trastuzumab model construction

Superposition of the crystal structures of domain fragments onto a template structure, referred to in this work as the KOL/Padlan structure (3,19), was accomplished using Swiss PDB viewer (20). The same software was also used to make mutations and add missing amino acids in the Fc domain so that its composition would be identical to that of the target antibody, trastuzumab. With the trastuzumab domains oriented relative to each other so that the coordinates of the template's hinge could be used to join the domains together, the PDB files for each domain and the hinge residues needed to complete the trastuzumab model were saved individually. Each PDB file's list of coordinate data was combined into a single file using a text editor. The protein and oligosaccharide residues were listed in the order of each chain's primary sequence so that the necessary peptide bonds would be made by AMBER's tleap (21) during topology/parameter building. AMBER's ff99 (22) and Glycam04 (23) force fields were used for the initial energy minimization and MD simulation trajectory.

MD simulations

For the initial T0 simulation, SANDER from the AMBER7 suite was used for the minimization, equilibration, and production dynamics. Energy minimization of the initial structure using generalized Born (GB) solvation was carried out to remove high-energy bonds and clashes that were artifacts of the model's construction process. The minimization procedure used 100 iterations of steepest descent followed by 100 iterations of conjugate gradient with an electrostatic cutoff of 12 Å and a solvent dielectric constant of 78. The system was solvated in an orthorhombic box of TIP3P water molecules with a 12 Å buffer of solvent between the solute's furthest dimensions in each direction. The result was a $167.4 \times 182.5 \times 92.5$ Å box that contained 74,577 water molecules and 12 chloride anions to make the system neutral.

An initial MD equilibration of the solvent was carried out with all protein and carbohydrate atoms restrained in a 50 kcal/mol energy well as the system was heated from 100 to 300 K over a period of 1.5 ps, with pressure held at 1 atm and taking 1 fs time steps for integration of atomic equations of motion. Next, six rounds of energy minimization on the entire system, each using 100 iterations of steepest descent followed by 100 iterations of conjugate gradient, were carried out with the restraints on the solute reduced in increments of 5 kcal/mol in each round from 25 kcal/mol in the first to 0 kcal/mol in the last. A final 20 ps MD equilibration followed in which the temperature of the system was increased from 100 K to 300 K. The density of the system increased from 0.8770 g/cm^3 to 0.9999 g/cm^3 during equilibration of the solvated system.

Production MD simulations with pressure and temperature held constant at 1 atm and 300 K were carried out from this point on. For this stage of simulation, the SHAKE algorithm was used and the size of the time steps for integrating the atomic equations of motion was increased to 2 fs. For each stage of equilibration and production dynamics once the system was solvated, the cutoff distance for calculating electrostatic interactions directly was set to 9 Å. Particle mesh Ewald summation was used to calculate electrostatic interactions beyond this distance. The cutoff for calculating van der Waals interactions was also set to 9 Å. An MD trajectory of 7.4 ns was computed with coordinates written to a file at 0.5 ps time intervals.

The potential energy of structures stripped of solvent and counterions was determined with AMBER's MM-PBSA script. The molecular mechanical energy of a structure, including the internal potential, nonbonded potential, and energy of solvation using the GB method, were determined with SANDER. An internal dielectric of one and a solvent dielectric of 80 were used for these calculations. No cutoff distances for nonbonded interactions were used.

Multiple MD simulations (T1–T8) were also carried out, with the following differences: The protein portion of the final structure of the initial trajectory was reparameterized with the improved parameter values of the ff99SB (24) force field, and parameters for the carbohydrates were again taken from the Glycam04 force field. The system was solvated in a truncated octahedral box of TIP3P water molecules with a 10 Å buffer of solvent between the solute's farthest dimensions in each direction. The result was a truncated octahedral box of water that contained 99,132 water molecules. The system was neutralized with 12 chloride ions. The final system contained 99,120 water molecules (297,360 atoms), 12 chloride ions, and 1348 residues of protein and sugar (20,692 atoms), which altogether amounts to a system with 318,064 atoms. The initial equilibration with solvent and preparation for production MD were achieved as described above for the T0 simulation.

At this point, eight parallel MD trajectories were started from the result of the previous steps using AMBER10's PMEMD. With the SHAKE algorithm applied and taking time steps of 2 fs, a 100 ps MD equilibration in which the temperature of the system was increased from 100 K to 315 K was carried out using different seed numbers for the randomization of atomic velocities in each of the eight trajectories. In the next 100 ps of MD equilibration, the temperature was cooled from 315 K to 300 K. Production MD simulations with pressure and temperature held constant at 1 atm and 300 K were carried out from this point on. Velocities of all atoms were again randomized at the start of the production dynamics and coordinates were written every 2 ps while each of the eight trajectories was run for 40 ns of simulation time. The van der Waals and electrostatic cutoffs were the same as for the T0 simulation.

Boundary element calculations

The methodology used for these calculations is discussed in detail in previous works (25–27). The modeling procedure used assumes that a 1.1 Å layer of water is uniformly distributed over the surface of the protein. The solvent-accessible surface of each structure was defined by MSROLL (28) using a 1.5 Å diameter ball rolled over the surface of the solute. This surface was triangulated by MSROLL using a fineness parameter value of 3.0. For the analysis of single structures only, the output of MSROLL, which contained ~40 k triangles for each of the full-length antibody structures studied in this work, was input to COALESCE (25) to produce five triangulations with ~9 k, 11.8 k, 12.5 k, 14.3 k, and 16 k triangles. The hydrodynamic boundary element program BEST (25–27) was used to compute the translational diffusion tensor, rotational diffusion tensor, and intrinsic viscosity of the molecules analyzed. The computed hydrodynamic properties, as a function of the inverse of the number of triangles, were plotted and fit to a straight line to extract the intercept, which is a precise value for the property corresponding to the smooth hydrodynamic surface. When 9 k or more triangles are used, the properties fall on a neat straight line, providing high-precision extrapolation to an infinite number of triangles.

For the analysis of an MD trajectory, coordinate files in PDB format were generated using the AMBER suite's ptraj program. PDB files with the trastuzumab model only were generated from each trajectory at 50 ps intervals. To avoid overrepresentation of the starting conformation, analysis of the first 10 ns of each trajectory was not included in the results reported. The solvent-accessible surface of each structure in the extracted PDB files was determined and tiled with triangles using MSROLL as described above. The resulting triangulations were processed by COALESCE to produce a single triangulation for each structure with ~9 k triangles. The transport properties for each structure were computed with BEST. Because of the large number of structures analyzed, the results were approximately extrapolated to an infinite number of triangles as described below and in Aragon and Hahn (26).

Determination of trastuzumab's translational diffusion coefficient by dynamic light scattering

For dynamic light scattering (DLS), a solution of trastuzumab was extensively dialyzed against a pH 7 solution of 20 mM NaP_i and 100 mM NaCl, maintained at 5°C. Five dilutions with concentrations in the range of 1–10 mg/mL were prepared and their concentrations were determined with an ultraviolet-visible spectrometer. For each sample, autocorrelation functions of fluctuations in the intensity of the 514.5 nm line of a Lexel 95 argon ion laser (Cambridge Lasers Laboratories Inc., Fremont, CA) scattered at a 90° angle from the solutions were determined by a Brookhaven Instruments (Holtsville, NY) BI-9000 AT digital autocorrelator and software that determined the mutual diffusion coefficient from the autocorrelation of the scattered intensity. The temperature of the samples was held constant to a tolerance of ±0.1°C with a Brinkmann (Metrohm USA, Riverview, FL) RM6 thermostated water bath.

The translational self-diffusion coefficient (D_t) for trastuzumab was obtained by extrapolating the values obtained for the mutual diffusion coefficient to zero concentration, as shown in Fig. 1. The self-diffusion coefficient obtained was adjusted using viscosity values for the buffer (1.013 mPa s) and water (1.002 mPa s) at 20°C so that the diffusion coefficient reported would correspond to trastuzumab in water at 20°C.

Measurements were carried out at 20°C and 27°C. The results obtained were found to agree to within 0.4% when scaled according to the Stokes-Einstein relation:

$$\frac{D_{t,20^\circ C}}{D_{t,27^\circ C}} = \frac{300K \times \eta_{H_2O,27^\circ C}}{293K \times \eta_{H_2O,20^\circ C}}$$

Results were obtained at two temperatures to confirm that the range of conformational space sampled at each temperature is not significantly different, and therefore it is acceptable to determine the transport property values for the antibody at 20°C by hydrodynamic modeling using structures generated with MD simulations run with a temperature of 300 K.

Determination of trastuzumab's intrinsic viscosity by dilute solution viscometry

A solution of trastuzumab was extensively dialyzed against a pH 7.4 solution of 20 mM KP_i and 100 mM KCl while it was kept at 5°C. Five dilutions with concentrations (c) in the range of 1–3 mg/mL were prepared. The viscosity of the buffer (η_0) and the viscosity of each dilution (η) was measured with an Anton Paar (Ashland, VA) SP3-V sample changer and AMVn rolling ball viscometer with temperature set to 20°C. The intrinsic viscosity $[\eta]$ of trastuzumab was determined as:

$$[\eta] = \lim_{c \to 0} \frac{\eta - \eta_0}{\eta_0 c}$$

RESULTS AND DISCUSSION

Model building

A complete crystal structure of trastuzumab, a humanized IgG1 antibody, does not exist. Therefore, to generate starting coordinates for this study, we obtained a crystal structure for

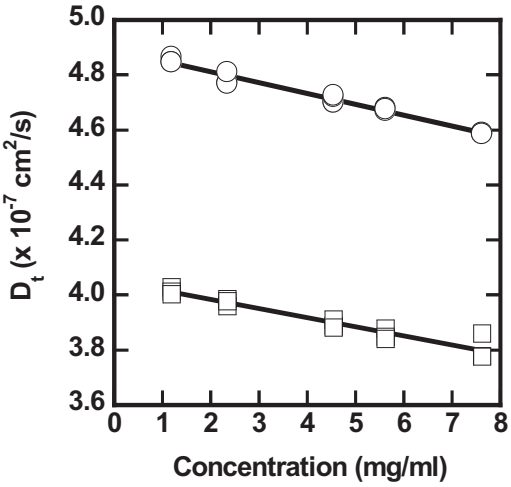

FIGURE 1 DLS extrapolations for the determination of trastuzumab's translational diffusion coefficient at 20°C (*squares*) and 27°C (*circles*); each measurement is in triplicate.

the Fab domain of trastuzumab, as well as the crystal structure for the G2-glycosylated Fc of a closely related antibody. To make this Fc fragment identical to that of the Fc of trastuzumab, mutations were made and missing residues added.

The structures available for use as references to obtain the starting coordinates for the 34 missing hinge residues (17 from each heavy chain (HC)) are limited in number. The PDB entries that contain potentially useful information include three full-length structures: human IgG1 b12 (6) (PDB entry 1HZH.pdb), mouse IgG1 61.1.3 (5) (PDB entry 1IGY.pdb), and mouse IgG2a 231 (4) (PDB entry 1IGT.pdb). Another PDB entry with information of interest is human IgG1 KOL (29) (PDB entry 1IG2.pdb), which forms crystals from which only the F(ab′)2 fragment (which includes both of the Fab domains and the upper and middle hinge residues) yields an interpretable electron density. The lower hinge and Fc domain of KOL do not appear in the Fourier map of electron density, most likely because the region adopts more than one conformation in its crystals.

The upper-hinge region of human IgG1 molecules contains a sequence (KTHT) that immediately precedes the middle-hinge region (3). In the KOL and b12 structures, this sequence forms a single-turn, open helix. However, b12 has the KTHT helix in only one of its upper-hinge HC strands and it is partially unwound, whereas the other strand does not yield an interpretable diffraction pattern for the THT region of the sequence. The KOL structure has a C2 symmetry axis that goes through the hinge and therefore has the KTHT helix in both of its HCs. We chose the KOL structure as the source of coordinates for the atoms of the upper- and middle-hinge regions, and as a template for orienting the Fab domains relative to each other. The coordinates for the atoms of the lower hinge of our starting structure were obtained from a hypothetical build of the region, assembled in silico by Padlan (3,19), to link the KOL F(ab′)2 (29) with a crystal structure of a human IgG1 Fc. This structure's hinge has the exact amino acid composition required to complete our model of trastuzumab. The ϕ/ψ dihedral angles of the lower hinge in space, as constructed by Padlan, are characteristic of β-sheets, which is consistent with the secondary structure composition of the majority of an IgG's structure (1,3). As shown below, the structure of the hinge region is well determined by the accurate force field used in this study, AMBER's ff99SB (22).

Electron microscopy studies (30) have indicated that IgGs populate many conformations, and fluorescence anisotropy studies (2) have indicated that IgGs possess segmental flexibility with internal motions that occur on a timescale of tens of nanoseconds. Therefore, if there do exist preferred conformations (e.g., such as that displayed by b12) with interdomain orientations or contacts that are preferred rather than a continuous range of equally probable conformations, it should be possible to observe relaxation into one or more of them within the timescale accessible in an MD simulation. Therefore, we decided it would be of interest to start our simulation from a slightly unnatural conformation, which likely would be ensured by using the theoretical lower hinge of the KOL/Padlan structure, so that it would be possible to observe relaxation into more favorable conformations.

MD simulations

Throughout the duration of the initial trajectory, the Fab and Fc domain structures appear to be very stable, as can be seen in a plot of their root mean-square deviation (RMSD; Fig. 2 *C*) using their initial coordinates as a reference. Although high-frequency vibrations are apparent throughout the structure, they are of relatively low amplitude. In comparison, the lower-hinge region appears to be quite flexible. The motions of this region appear to be larger in amplitude, which is not unexpected since there is no secondary structure in this region and it is highly exposed to solvent. On the other hand, the Fab domains initially reorient slightly relative to each other, but otherwise appear to move as a single unit. About 1.5 ns into the trajectory, the Fc domain rotates ~45° about its long axis and begins to drift toward one of the Fabs. At ~5 ns into the trajectory, another conformational change begins that results in the upper hinge bending so that the molecule adopts a slightly trigonal pyramidal shape rather than the trigonal planar shape of the starting conformation. Correlations to the two largest-scale motions noted above are apparent in a plot of the entire structure's RMSD (Fig. 2 *C*). A large shift is observed in the first 2–3 ns, which is likely due to the movement of the Fc and lower hinge. The structure then stays roughly in that conformation until ~5 ns into the trajectory, which is consistent with the plateau in the value of the RMSD during this period. At ~5.5 ns, a shift in the RMSD occurs that corresponds well with the conformational shift that results in the upper hinge bending.

The plateau in the value of the entire structure's RMSD is a possible indication that the high potential energy artifacts due to interdomain contacts or orientations present in the initial coordinates have been relaxed (31). A molecular mechanics (MM) analysis of structures from along the trajectory confirms that the model has descended into an energy basin on its potential energy surface (Fig. 2 *D*). To test whether the drop in potential energy could be due to relaxation of the domains rather than relaxation of interdomain orientation and interactions, we ran a simulation of the trastuzumab Fab alone, using the same parameters and conditions as for the initial trastuzumab simulation, and analyzed it using the same method employed for the whole trastuzumab simulation. There was no comparable relaxation in potential energy for the Fab-only simulation (Fig. 2 *E*).

A hydrodynamic analysis of the starting ($\text{Trastuzumab}_{\text{T0,t=0}}$) and final ($\text{Trastuzumab}_{\text{T0,t=7.4}}$) structures indicates that the final structure has properties in closer agreement with experimentally determined, ensemble-averaged hydrodynamic measurements (Table 1). Therefore, the structure that results

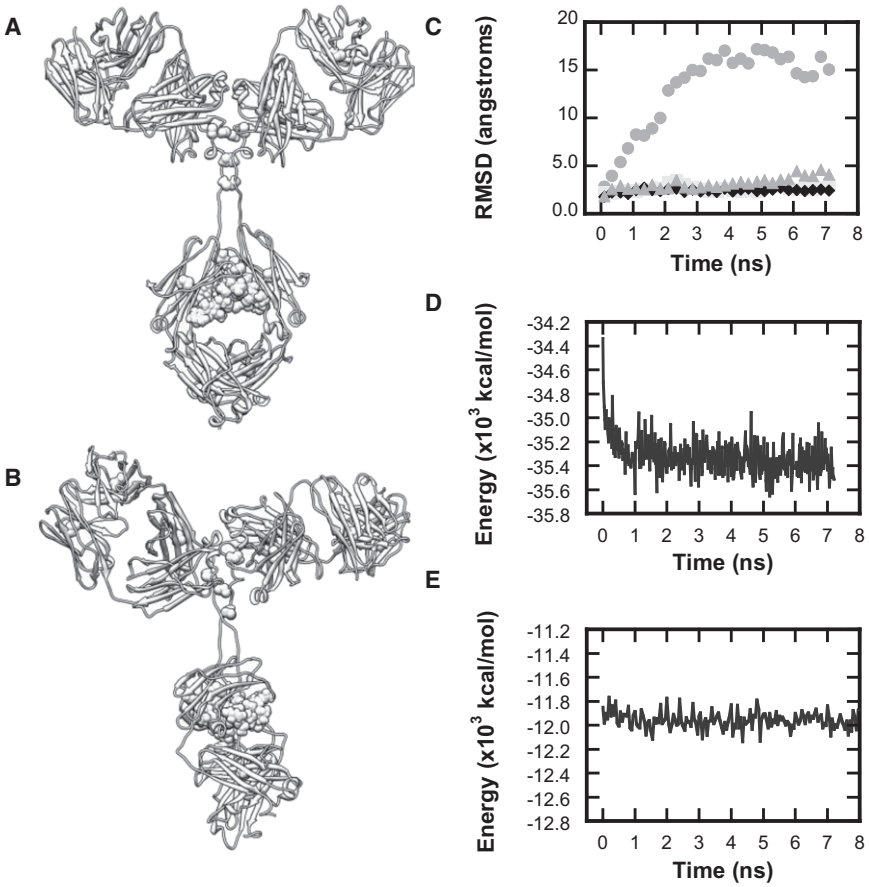

FIGURE 2 (*A*) Trastuzumab (T0,t=0). (*B*) Trastuzumab at t=7.4 ns of simulation T0. (*C*) RMSD, during initial trajectory, of the trastuzumab model as a whole (*circles*), Fab1 (*diamond*), Fab2 (*square*), and Fc (*triangle*). (*D*) MM-GBSA analysis of the trastuzumab model during initial trajectory. (*E*) MM-GBSA analysis of the trastuzumab Fab-only simulation; molecular graphics produced with UCSF Chimera (33).

from the initial trajectory is most likely more characteristic of an antibody in solution than is the conformation of the initially pieced-together structure.

To maximize the amount of conformational space sampled (32), eight further simulation trajectories were generated in parallel, with the relaxed trastuzumab model used as the initial conformation for each. The motions observed in the 7.4 ns trajectory indicated that a larger simulation cell is required to ensure that the model does not interact with an image of itself. Visual inspection of these eight 40-ns trajectories (Movie S1 in the Supporting Material) clearly reveals distinct explorations of simulation phase space. Though the same starting structure was used for each trajectory, the use of different seed numbers for the randomization of atomic velocities during temperature and pressure equilibration of each system and at the outset of production dynamics was sufficient to send each antibody structure onto unique pathways in conformational space.

In the hierarchy of motions in the trajectories, the rotation of the Fc relative to the Fab domains appears to be the fastest of the large domain motions. A slightly slower domain motion is present in the translational diffusion of the Fc relative to the Fab domains. The Fab-Fc angle is observed at angles ranging from nearly 0 to 180°. Of the domain-domain reorientation motions observed, that between the Fab domains changes on the slowest timescale during the length of our simulations. In fact, on short timescales, the Fab domains appear to behave as a single F(ab)2 unit. When observed over a longer timescale and multiple trajectories, however, it is clear that the two domains' orientation to one another does change, primarily by rotation about non-shared axes that are ~140° apart and cross roughly at the point where the two Fab domains are closest.

TABLE 1 Hydrodynamic modeling results for single structures, and summary of our experimental hydrodynamic results and results from the literature

Antibody	D_t ($\times 10^7$ cm^2/s)*	τ_r (ns)†	$[\eta]$ (cm^3/g)
b12 (1hzh.pdb) (6)	4.021 (±0.009)	183.4 (±0.4)	6.425 (±0.005)
61.1.3 (1igt.pdb) (4)	3.966 (±0.003)	191.5 (±0.0)	6.681 (±0.004)
213 (1igy.pdb) (5)	4.221 (±0.002)	157.6 (±0.0)	5.662 (±0.002)
KOL/Padlan (17)	3.873 (±0.002)	213.9 (±0.5)	7.275 (±0.004)
Trastuzumab (T0,t=0)	3.989 (±0.008)	192.0 (±0.2)	6.739 (±0.003)
Trastuzumab (T0,t=7.4)	4.006 (±0.002)	187.3 (±0.4)	6.277 (±0.005)
Trastuzumab experiment	4.09 (±0.01)		6.37 (±0.2)
IgG literature‡		168 (2), 180 (38)	6.20 (±0.5) (39)

All values correspond to a temperature of 20°C in pure water.
*For computational results: $D_t = 1/3\ \mathrm{Tr}(D_{tt})$.
†For computational results: $\tau_r = (6D_r)^{-1}$, where $D_r = 1/3\ \mathrm{Tr}(D_{rr})$.
‡Experimental results for rabbit IgG (2), bovine IgG (38), and human IgG1 (39).

The Fab-Fab orientation in our model seems to be strongly influenced by these domains' contact with each other above the hinge region. During the course of the eight 40-ns simulation trajectories, the two domains are rarely out of contact with each other. The region in which the Fab domains make contact with each other is rich in aspartate, glutamate, and lysine residues. Therefore, it is likely that the interaction observed between the Fab domains is stabilized by electrostatic forces. This interaction could be prevalent in the multiple trajectories simply because it is common to all of the conformational space that is locally accessible from the starting structure. We address the question of whether the conformations observed in the simulations could be representative of a human IgG1 in solution at length in the following sections.

Computation of hydrodynamic transport properties

We applied hydrodynamic modeling in this study to evaluate our MD results. We first analyzed a set of single structures to see how close they were to experimental values, and then computed the transport properties as ensemble averages over full MD trajectories.

Computational hydrodynamic analyses of single structures, in which a single structure is triangulated multiple times with a range of triangle numbers and the results are extrapolated to an infinite number of triangles, were carried out on each of the full-length antibody structures in the PDB (61.1.3, 231, and b12) as well as the KOL/Padlan structure and the trastuzumab model structure from the T0 trajectory in its initial ($\text{Trastuzumab}_{\text{T0,t=0}}$; Fig. 2 *A*) and final ($\text{Trastuzumab}_{\text{T0,t=7.4}}$; Fig. 2 *B*) conformations. We compared the experimental diffusion coefficients with the average of the three eigenvalues of the corresponding tensors. To obtain the rotational correlation time, we used the approximate formula $\tau_r = (6D_r)^{-1}$. Fig. 3 and Fig. S1 show that the three eigenvalues of the rotational diffusion tensor typically differ only ~25–20% from their average; thus, any kind of specific weighting by a particular measurement technique will yield a value very close to the above rotational correlation time. The close agreement with experiment (Table 2) corroborates this assertion.

The results computed for the initial and final snapshots from our simulation T0 and whole antibody crystal structures in the PDB are summarized in Table 1. The structure that yields the least agreement to experimental data is the KOL/Padlan structure, which was chosen as a source of hinge coordinates and as a template for the initial interdomain orientations of the trastuzumab model. The transport properties of our model's initial structure ($\text{Trastuzumab}_{\text{T0,t=0}}$) are in slightly better agreement with experimental values, possibly due to the different elbow angle of the Fab domains or the slightly closer proximity of the Fab domains to each other relative to the Fab domains in the KOL/Padlan structure. However, the final structure of the initial trajectory ($\text{Trastuzumab}_{\text{T0,t=7.4}}$), which is also the starting structure for the multiple trajectories (T1–T8), matches experimental values quite well. The best match comes from the human IgG1 b12 structure (6). It is notable that both our $\text{Trastuzumab}_{\text{T0,t=7.4}}$ model and b12 both match very well with experimental values and yet have very different interdomain orientations. Given the flexibility we expect in an antibody structure (2,34), the single molecule results were included only to provide a frame of reference and to

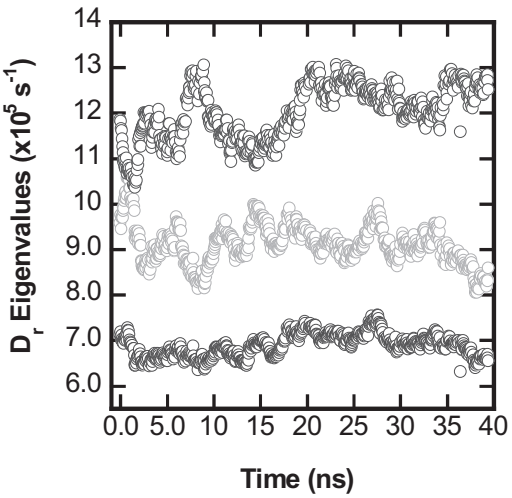

FIGURE 3 Plots of the eigenvalues of the rotational diffusion tensor, D_r, of structures from simulation T5; Fig. S1 has corresponding plots for all simulation trajectories T1–T8.

TABLE 2 Summary of hydrodynamic analysis of MD simulation data, our experimental hydrodynamic results, and results from the literature

Trajectory	D_t ($\times 10^{-7}$ cm^2/s)*†	τ_r (ns)‡†	$[\eta]$ (cm^3/g)†
1	4.00 (±0.04)	184 (± 9)	6.6 (±0.2)
2	4.12 (±0.05)	168 (± 8)	6.0 (±0.3)
3	4.15 (±0.06)	158 (± 10)	6.1 (±0.3)
4	3.97 (±0.03)	190 (± 5)	6.7 (±0.1)
5	4.05 (±0.03)	179 (± 5)	6.4 (±0.2)
6	4.11 (±0.03)	168 (± 5)	6.0 (±0.1)
7	4.17 (±0.07)	164 (± 10)	5.9 (±0.4)
8	4.09 (±0.04)	172 (± 8)	6.2 (±0.2)
Average§	4.08 (± 0.07)	173 (± 11)	6.24 (± 0.3)
Experiment¶	4.09 (± 0.01)		6.37 (± 0.2)
Literature‖		168 (2), 180 (38)	6.20 (±0.5) (39)

All values correspond to a temperature of 20°C in pure water.
*For computational results: $D_t = 1/3\ \text{Tr}(D_{tt})$.
†For individual trajectories; the value quoted is the trajectory average and its standard deviation.
‡For computational results: $\tau_r = (6D_r)^{-1}$, where $D_r = 1/3\ \text{Tr}(D_{rr})$.
§Values quoted are the average of each trajectory's average and their standard deviation.
¶See Methods and Materials; uncertainties quoted are the standard error of extrapolations to $c = 0$.
‖Experimental values for rabbit IgG (2), bovine IgG (38), and human IgG1 (39).

demonstrate that the initial trajectory's final conformation is more likely characteristic of an antibody in solution than is its initial state.

Many proteins and protein complexes can reasonably be treated as rigid bodies in computations of their hydrodynamic properties (26,27). By performing boundary-element calculations on structures taken at regular intervals from along an MD trajectory and averaging them, one can obtain values for a flexible molecule. The ensemble average over rigid bodies approach to modeling flexible bodies has a long history. In a study of flexible dumbbells, Zimm (35) demonstrated that the error in the approximation is very small. Hagerman and Zimm (36) used this approach to provide the first expressions for the rotational diffusion coefficients of semiflexible polymers. Fixman (37) and others demonstrated that the method is exact for the pre-averaged hydrodynamic interaction, and thus the difference between the fluctuating hydrodynamic interaction and the rigid body ensemble approach is very small when full hydrodynamic interactions are included. Furthermore, as long as the force field used is sufficiently accurate, appropriate simulation parameters are applied, and the simulations sample sufficient conformational space, the collection of structures that an MD simulation produces will be representative of a Boltzmann-weighted ensemble. In the work presented here, >6000 structures were used to compute the ensemble average transport properties.

Computing the hydrodynamic properties of the thousands of structures extracted from MD trajectories and extrapolating each to an infinite triangle number (25) is very time-consuming. Therefore, we used the average slope from a full extrapolation to an infinite number of triangles of each trajectory's last structure to extrapolate each transport property to the smooth surface. This is quite a good approximation since the extrapolation correction amounts to within only 0.5%, 1.0%, and 1.6% of the value of D_t, D_r, and $[\eta]$, respectively. The scaled results of the hydrodynamic trajectory analyses are plotted for each trajectory in Fig. 4 and Fig. S1, and their averages are summarized in Table 2.

The average D_t value at 293 K over all of the trajectories is $4.08\times10^{-7} \pm 0.07\times10^{-7}$ cm^2/s, which is within 0.3% of the value determined with DLS ($4.09\times10^{-7} \pm 0.03\times10^{-7}$ cm^2/s). The average D_r value at 293 K over all of the trajectories is $9.58\times10^5 \pm 0.6\times10^5$ s^{-1}, which corresponds to a rotational correlation time (τ_r), according to the relationship $\tau_r = (6\,D_r)^{-1}$, of 174 ± 11 ns. This value is within 3.6% of the value given in the literature for the rotational correlation time of a rabbit IgG (168 ns) as determined by fluorescence anisotropy (2) at 20°C, and within 3.3% of the value reported for the rotational correlation time of a bovine IgG (180 ns) as determined by electric birefringence (38) at 20°C. The value computed from the trajectories for the average intrinsic viscosity is 6.24 ± 0.30 cm^3/g, which is within 0.7% of the value given for a human IgG1 at 20°C (6.20 ± 0.50 cm^3/g (39)), and within 3.0% of the value

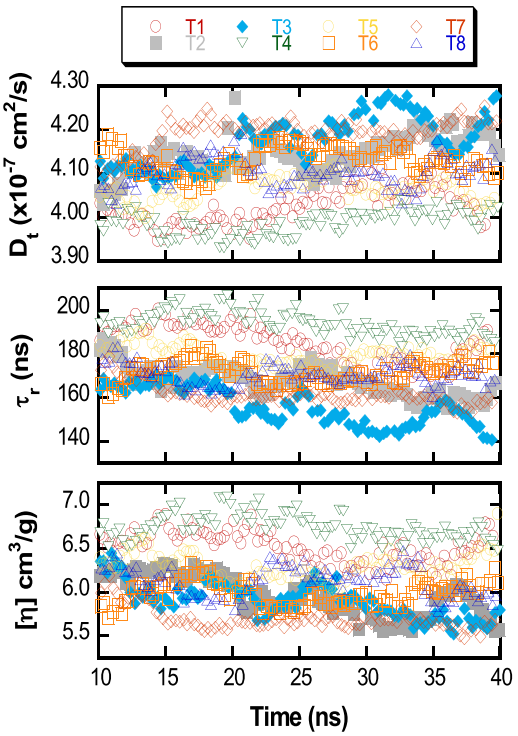

FIGURE 4 Plots of hydrodynamic analysis results; values are adjusted for each transport property using the average slope obtained from full hydrodynamic analysis of the trajectories' last structure. Note: The density of the data points displayed is 20% of each trajectory's data included in the numerical data presented in Table 2.

we determined for trastuzumab at 20°C (6.37 ± 0.19 cm^3/g). These values are summarized in Table 2. The computed values are stated for pure water at the temperature cited, whereas the experimental data have been corrected to pure water using the viscosity of the buffer solution.

The excellent agreement between the computational hydrodynamic analysis of the collection of MD trajectories and our determinations for the translational diffusion coefficient and intrinsic viscosity of trastuzumab samples, as well as with literature values for the translational diffusion coefficient, rotational correlation time, and intrinsic viscosity of IgG molecules, strongly supports our contention that the range of conformations observed in the MD simulations represents the solution conformations undertaken by trastuzumab molecules in the range of 293–300 K. The data show that the rigid ensemble approach to the computation of properties of flexible antibodies works very well.

CONCLUSIONS

In this work, we describe the successful generation of MD trajectories for a model of a human IgG1 antibody that was assembled from domain fragments, only one of which had the exact amino acid composition of the target molecule. Our model-building choices were guided by the assumption that the crystal structures of whole antibodies that are

available in the PDB most likely have some exceptional feature that makes them crystallizable, and therefore are not necessarily the best templates to use in building our model structure. Therefore, we chose to use the KOL/Padlan structure, which features a hinge built in silico, as our template. MM analysis of our initial trajectory (T0) revealed that the model relaxed during a 7.4 ns simulation (Fig. 2 *D*). When these results are compared with those obtained in a Fab domain-only simulation (Fig. 2 *E*), it is clear that the domains themselves are not the source of the relaxation. Therefore, we conclude that shifts in the interdomain orientation within the model are the source of the lower potential energy of the resulting structure. In the multiple trajectories that were started with the result of the initial trajectory as their starting conformation, we observe a wide range of conformations.

To assess whether the structures generated could be representative of trastuzumab in solution, we analyzed structures taken at regular intervals from each simulation trajectory with BEST (25–27), a very precise and accurate boundary-element, hydrodynamic modeling technique, and compared the results with values obtained from our measurements of samples of trastuzumab and values found in the literature for IgG molecules. We find that the trajectory transport property averages agree extremely well with values obtained experimentally. Therefore, given the precision and accuracy of the hydrodynamic method used to evaluate the simulation results, we are able to conclude that the collection of structures generated in the multiple MD trajectories is a good representation of the conformations achieved by antibodies in aqueous solution. It should be noted, however, that the kinetics of the motions observed are not expected to be accurate, due to the limited accuracy of the water model used (40). Since the TIP3P water model underestimates the viscosity of water, the motions are all faster than would be expected in true water. However, the advantage of hydrodynamic modeling is that we only need accurate conformations, not the precise timing of the motions. Thus, trajectories that are much shorter than needed to extract the full dynamic correlation functions can be successfully used to compute measurable hydrodynamic properties. Our data show that the force field used and the simulation parameters employed sufficiently represent the structure and dynamics of trastuzumab, and therefore its hydrodynamic properties are accurately reproduced.

In this work, extremely good agreement between measurement and computation was achieved because the physical samples of trastuzumab were fabricated for pharmaceutical purity; the measurements were carried out to very high precision with DLS; the simulation used explicit water, a realistic force field, and all-atom detail for the protein and sugars on the Fc region; and the hydrodynamic computations were high-precision, boundary-element computations that used a large number of surface elements for the definition of molecular shape.

As mentioned above, one previously reported study also used an all-atom MD simulation to explore the solution phase properties of whole antibody structure (15,16). However, to our knowledge, the MD simulations reported here are the first simulations of a whole antibody to be validated against experimental measurements that are sensitive to the overall conformational features of molecules in solution. The agreement of our simulation results with experimental determinations of the hydrodynamic properties of the molecule modeled suggests that the methodology used to construct our model and the simulation parameters applied are reasonably good choices and should have broad applicability across antibody classes. Likewise, these results suggest that the combination of modeling and experiments used may also be useful for investigating the solution phase properties of similar antibodies or other flexible molecules.

SUPPORTING MATERIAL

One figure, one movie, and two structure files are available at http://www.biophysj.org/biophysj/supplemental/S0006-3495(10)00565-5.

The authors thank Trevor E. Swartz and Jamie Moore for establishing collaboration between Genentech and San Francisco State University, and for helpful discussions. The authors also thank David Konerding and Nevin Cheung of Genentech for technical support.

This work was partially supported by National Institutes of Health grant GM52588 to S.R.A.

REFERENCES

1. Noelken, M. E., C. A. Nelson, …, C. Tanford. 1965. Gross conformation of rabbit 7 S γ-immunoglobulin and its papain-cleaved fragments. *J. Biol. Chem.* 240:218–224.
2. Yguerabide, J., H. F. Epstein, and L. Stryer. 1970. Segmental flexibility in an antibody molecule. *J. Mol. Biol.* 51:573–590.
3. Padlan, E. A. 1994. Anatomy of the antibody molecule. *Mol. Immunol.* 3:169–217.
4. Harris, L. J., S. B. Larson, …, A. McPherson. 1992. The three-dimensional structure of an intact monoclonal antibody for canine lymphoma. *Nature.* 360:369–372.
5. Harris, L. J., E. Skaletsky, and A. McPherson. 1998. Crystallographic structure of an intact IgG1 monoclonal antibody. *J. Mol. Biol.* 275:861–872.
6. Saphire, E. O., P. W. Parren, …, I. A. Wilson. 2001. Crystal structure of a neutralizing human IGG against HIV-1: a template for vaccine design. *Science.* 293:1155–1159.
7. Guddat, L. W., J. N. Herron, and A. B. Edmundson. 1993. Three-dimensional structure of a human immunoglobulin with a hinge deletion. *Proc. Natl. Acad. Sci. USA.* 90:4271–4275.
8. Yu, H. 1999. Extending the size limit of protein nuclear magnetic resonance. *Proc. Natl. Acad. Sci. USA.* 96:332–334.
9. Boehm, M. K., J. M. Woof, …, S. J. Perkins. 1999. The Fab and Fc fragments of IgA1 exhibit a different arrangement from that in IgG: a study by X-ray and neutron solution scattering and homology modelling. *J. Mol. Biol.* 286:1421–1447.
10. Furtado, P. B., P. W. Whitty, …, S. J. Perkins. 2004. Solution structure determination of human IgA2 by X-ray and neutron scattering and analytical ultracentrifugation and constrained modeling: a comparison with human IgA1. *J. Mol. Biol.* 338:921–941.

11. Sun, Z., A. Almogren, …, S. J. Perkins. 2005. Semi-extended solution structure of human myeloma immunoglobulin D determined by constrained X-ray scattering. *J. Mol. Biol.* 353:155–173.
12. Longman, E., K. Kreusel, …, S. E. Harding. 2003. Estimating domain orientation of two human antibody IgG4 chimeras by crystallohydrodynamics. *Eur. Biophys. J.* 32:503–510.
13. Lu, Y., E. Longman, …, S. E. Harding. 2006. Crystallohydrodynamics of protein assemblies: Combining sedimentation, viscometry, and x-ray scattering. *Biophys. J.* 91:1688–1697.
14. Lu, Y., S. E. Harding, …, J. García de la Torre. 2007. Solution conformation of wild-type and mutant IgG3 and IgG4 immunoglobulins using crystallohydrodynamics: possible implications for complement activation. *Biophys. J.* 93:3733–3744.
15. Chennamsetty, N., B. Helk, …, B. L. Trout. 2009. Aggregation-prone motifs in human immunoglobulin G. *J. Mol. Biol.* 391:404–413.
16. Chennamsetty, N., V. Voynov, …, B. L. Trout. 2009. Design of therapeutic proteins with enhanced stability. *Proc. Natl. Acad. Sci. USA.* 106:11937–11942.
17. Carter, P., L. Presta, …, H. M. Shepard. 1992. Humanization of an anti-$p185^{HER2}$ antibody for human cancer therapy. *Proc. Natl. Acad. Sci. USA.* 89:4285–4289.
18. Goldenberg, M. M. 1999. Trastuzumab, a recombinant DNA-derived humanized monoclonal antibody, a novel agent for the treatment of metastatic breast cancer. *Clin. Ther.* 21:309–318.
19. Atomic Coordinate Files for Whole IgG1. http://www.umass.edu/microbio/rasmol/padlan.htm. Accessed June 2, 2008.
20. Guex, N., and M. C. Peitsch. 1997. SWISS-MODEL and the Swiss-PdbViewer: an environment for comparative protein modeling. *Electrophoresis.* 18:2714–2723.
21. Perlman, D. A., D. A. Case, …, P. Kollman. 1995. AMBER, a package of computer programs for applying molecular mechanics, normal mode analysis, molecular dynamics and free energy calculations to simulate the structural and energetic properties of molecules. *Comput. Phys. Commun.* 91:1–41.
22. Wang, J., P. Cieplak, and P. A. Kollman. 2000. How well does a restrained electrostatic potential (RESP) model perform in calculating conformational energies of organic and biological molecules? *J. Comput. Chem.* 21:1049–1074.
23. Kirschner, K. N., A. B. Yongye, …, R. J. Woods. 2008. GLYCAM06: a generalizable biomolecular force field. Carbohydrates. *J. Comput. Chem.* 4:622–655.
24. Hornak, V., R. Abel, …, C. Simmerling. 2006. Comparison of multiple Amber force fields and development of improved protein backbone parameters. *Proteins.* 65:712–725.
25. Aragon, S. R. 2004. A precise boundary element method for macromolecular transport properties. *J. Comput. Chem.* 25:1191–1205.
26. Aragon, S., and D. K. Hahn. 2006. Precise boundary element computation of protein transport properties: diffusion tensors, specific volume, and hydration. *Biophys. J.* 91:1591–1603.
27. Hahn, D. K., and S. R. Aragon. 2006. Intrinsic viscosity of proteins and platonic solids by boundary element methods. *J. Chem. Theory Comput.* 2:1416–1428.
28. Connolly, M. L. 1983. Analytical molecular surface calculation. *J. Appl. Cryst.* 6:548–558.
29. Huber, R., J. Deisenhofer, …, W. Palm. 1976. Crystallographic structure studies of an IgG molecule and an Fc fragment. *Nature.* 264:415–420.
30. Roux, K. H., and D. W. Metzger. 1982. Immunoelectron microscopic localization of idiotypes and allotypes on immunoglobulin molecules. *J. Immunol.* 129:2548–2553.
31. Walton, E. B., and K. J. Vanvliet. 2006. Equilibration of experimentally determined protein structures for molecular dynamics simulation. *Phys. Rev. E Stat. Nonlin. Soft Matter Phys.* 74:061901.
32. Caves, L. S. D., J. D. Evanseck, and M. Karplus. 1998. Locally accessible conformations of proteins: multiple molecular dynamics simulations of crambin. *Protein Sci.* 7:649–666.
33. Pettersen, E. F., T. D. Goddard, …, T. E. Ferrin. 2004. UCSF Chimera—a visualization system for exploratory research and analysis. *J. Comput. Chem.* 25:1605–1612.
34. Bongini, L., D. Fanelli, …, U. Skoglund. 2004. Freezing immunoglobulins to see them move. *Proc. Natl. Acad. Sci. USA.* 101:6466–6471.
35. Zimm, B. H. 1982. Sedimentation of asymmetric elastic dumbbells and the rigid-body approximation in the hydrodynamics of chains. *Macromolecules.* 15:520–525.
36. Hagerman, P. J., and B. H. Zimm. 1981. Monte-Carlo approach to the analysis of the rotational diffusion of wormlike chains. *Biopolymers.* 20:1481–1502.
37. Fixman, M. 1981. Symmetry criteria in the theory of chain polymer hydrodynamics. *Macromolecules.* 14:1706–1709.
38. Riddiford, C. L., and B. R. Jennings. 1967. Kerr effect study of the aqueous solutions of three globular proteins. *Biopolymers.* 5:757–771.
39. Kilár, F., I. Simon, …, P. Závodszky. 1985. Conformation of human IgG subclasses in solution. Small-angle X-ray scattering and hydrodynamic studies. *Eur. J. Biochem.* 147:17–25.
40. Horn, H. W., W. C. Swope, …, T. Head-Gordon. 2004. Development of an improved four-site water model for biomolecular simulations: TIP4P-Ew. *J. Chem. Phys.* 120:9665–9678.